Int. J. Heat Mass Transfer. Vol. 35, No. 7, pp. 1795–1801, 1992
Printed in Great Britain

0017-9310/92 $5.00 + 0.00

Thermal transport in polystyrene and polyurethane foam insulations

J. KUHN, H.-P. EBERT, M. C. ARDUINI-SCHUSTER, D. BÜTTNER and J. FRICKE
Physikalisches Institut der Universität, Am Hubland, D-8700 Würzburg, Germany

(*Received* 13 *February* 1991)

Abstract—The thermal transport in polystyrene (PS) and polyurethane (PU) foam insulations is described, with special emphasis on the radiative transfer. Calorimetric measurements of the total conductivity are performed in a guarded hot-plate device. The radiative properties of the foams are derived from infrared-optical investigations with an FTIR spectrometer. In the case of the PS foam, radiative properties are also extracted from calculations using the Mie scattering theory for infinite cylinders and platelets, representing the struts and walls of the foam cells, respectively. The total thermal conductivity of PU foams, including condensation effects of the blowing agent R 11, is modelled.

1. INTRODUCTION

INSULATING foams consist of a highly porous but coherent solid body with a cellular structure. Heat transport occurs via gaseous and solid thermal conduction as well as radiative transfer [1]. The gaseous conductivity depends on the composition of the trapped gas, which changes with time by infusion of atmospheric gases and to some extent also by effusion and condensation of the blowing agent [2, 3]. The solid conductivity depends on the cellular structure, consisting of struts and cell walls (Fig. 1). During the foaming process the struts are the material reservoir, from which the growing cell walls are supplied. The conductive process within these structures can be described using a simple cubic model [1]. Attenuation of thermal radiation occurs via scattering and absorption by the struts and walls. Theoretically the radiative transfer can be described by the Mie scattering theory for cylinders [4] and platelets [5]. Extinction data are also derived by infrared (ir)-optical directional-hemispherical transmission and reflection measurements.

Coupling effects, which may occur between the heat transfer modes [6], are negligible for foams [7]. Gaseous and solid thermal conduction have no influence on each other as localized high thermal resistances are not present in the coherent foam structure. Furthermore, the ir-optical thickness is around 20 for 1-cm-thick specimens; thus coupling between solid and radiative conductivity can be neglected.

Convection does not occur in foams either [2, 8], as the cells are sufficiently small and the modified Rayleigh numbers are thus far below the critical values.

The total thermal conductivity λ of foams is thus determined by linear superposition [1, 2] of the solid, gaseous and radiative conductivity, λ_s, λ_g and λ_r, respectively:

$$\lambda = \lambda_s + \lambda_g + \lambda_r. \tag{1}$$

An experimental separation of these contributions is a non-trivial task, as foams—always containing a certain fraction of closed cells—cannot be fully evacuated. The separation is still achievable, if suitable models are employed and caloric measurements are combined with ir-optical measurements. Such a separation is important for a systematic enhancement of the total thermal resistance. The goal of this paper is the detailed investigation of a polystyrene (PS) and a polyurethane (PU) foam and the separation of the thermal transfer modes. In particular the radiative transfer is studied theoretically and experimentally.

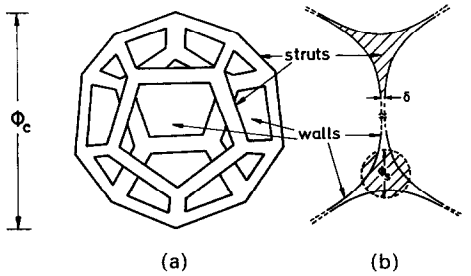

FIG. 1. Dodecaeder model for a foam cell. (a) Perspective view. (b) Cross-section through struts and walls [16].

2. DESCRIPTION OF STRUCTURE AND THERMAL TRANSPORT

2.1. *Solid conduction*

The foaming process leads to the formation of cells which resemble regular pentagonal dodecahedrons (Fig. 1) [1]. An average cell diameter ϕ_c, an effective strut diameter ϕ_s and a mean wall thickness δ can be derived from SEM pictures considering orientation effects [8]. These data allow one to determine the mass fractions $m_s/(m_w+m_s)$ and $m_w/(m_w+m_s)$ of struts and walls, respectively. The following equations con-

NOMENCLATURE

d	collision radius, $d_{ik} = r_i + r_k$	Λ	wavelength
e	specific extinction	ρ	density
f	mass fraction	σ	Stefan–Boltzmann constant
k	imaginary part of $m(\Lambda)$	ϕ	diameter
$m(\Lambda)$	spectral complex index of refraction: $m(\Lambda) = n + ik$	ω	albedo.
m	mass	Subscripts	
n	real part of $m(\Lambda)$	c	cell
p	partial gas pressure	g	gaseous
Q	relative extinction cross-section	m	mean
R	reflection	N	nitrogen
r	radius of a molecule	R	Rosseland-averaged
T	transmission.	r	radiative
		s	strut, solid
Greek symbols		w	wall
α	angle	0	bulk material
γ	geometrical coefficient	1, 2	type of gas.
δ	wall thickness		
Θ	temperature	Superscript	
λ	thermal conductivity	*	effective.

taining the geometrical proportions of the dodecahedron are then used:

$$m_s/\rho_0 = 2.8\phi_c\phi_s^2 - 3.9\phi_s^3 \tag{2}$$

$$m_w/\rho_0 = \{1.3\phi_c^2 - 5.4\phi_c\phi_s + 1.7\phi_s^2\}\delta \tag{3}$$

where ρ_0 is the density of the bulk material. Typically we find for the mass fraction of the struts

$$f_s = \frac{m_s}{m_w + m_s} \approx 0.6\text{–}0.9 \tag{4}$$

in accordance with ref. [1].

To determine the solid conductivity, a simple cubic model can be used [1], where parts of the structural elements are either taken parallel or vertical to the macroscopic temperature gradient. The mass fraction of struts and walls, derived from the dodecaeder model, are also applied in the cubic model. This allows one to determine the geometry of a cube with the same characteristics for thermal transport as the dodecahedron. If one assumes that two-thirds of the walls and one-third of the struts are oriented parallel to the temperature gradient, the solid conductivity of the foam is given by

$$\lambda_s = (2/3 - f_s/3) \cdot \rho/\rho_0 \cdot \lambda_0 \tag{5}$$

where ρ and ρ_0 are the densities of the foam and the bulk material, respectively; λ_0 is the solid conductivity of the bulk material.

For typical PU foams, values of $f_s \approx 0.7$, $\lambda_0 \approx 0.26$ W m^{-1} K^{-1} and $\rho/\rho_0 \approx 0.04$ give a solid conductivity $\lambda_s \approx 0.004$ W m^{-1} K^{-1}.

2.2. *Gaseous conduction*

The small gaseous conductivity in CFC-blown insulating foams is due to the large molecular mass of the blowing agent; if gas-tight surface covers are employed, a considerable fraction of the blowing gas may be retained in the cells during the lifetime of the insulation. The outgassing CFC fraction in any case contributes toward ozone depletion in the upper atmosphere.

Infusion of atmospheric gases occurs to a much larger extent. This leads to a noticeable increase of total gaseous conduction in the cells within weeks and months. The diffusion coefficients for CO_2 and N_2 are larger than those for R 11 (CCl_3F) by roughly a factor of 400 and 20, respectively [9]. The thermal conductivities of the atmospheric gases N_2 and O_2 are at least three times higher than for R 11 (0.008 W m^{-1} K^{-1}).

The conductivity of the gas mixture can be estimated from a linear superposition of the ingredients, weighted by their partial pressures. A more accurate derivation has to consider the collision cross-sections and the masses m_i of the involved molecules. For a two-component gas mixture, the conductivity in our case is sufficiently well described by the following equation (cf. ref. [10]):

$$\lambda_{mix} = \frac{\lambda_{gas,1}}{1 + \frac{p_2}{p_1}\left[\frac{d_{12}}{d_{11}}\right]^2 \sqrt{\left(\frac{m_1+m_2}{2m_2}\right)}} + \frac{\lambda_{gas,2}}{1 + \frac{p_1}{p_2}\left[\frac{d_{12}}{d_{22}}\right]^2 \sqrt{\left(\frac{m_1+m_2}{2m_1}\right)}} \tag{6}$$

where p_1 and p_2 are the partial pressures of the gases and d_{ik} is the sum of the radii of two colliding molecules i and k. If the d_{ik} are not available, their ratio can be expressed in terms of viscosity, gas density and average velocity of the gas molecules.

The increase of λ_{mix} of an R 11/nitrogen mixture with partial nitrogen pressure p_N is shown in Fig. 2. For low initial R 11 pressures the increase in λ_{mix} with p_N is around 0.015 W m^{-1} K^{-1}, if the N_2 pressure rises by a few hundred mbar.

For $p_{R11} = 0.5$ bar λ_{mix} rises by only 0.010 W m^{-1} K^{-1}. Typical CFC-blown foams for applications show gaseous conductivities of about 0.018 W m^{-1} K^{-1} after an aging period of 2 months.

2.3. *Radiative conductivity*

The described strut/wall structure contributes considerably to the attenuation of thermal radiation and thus to the effective specific extinction e^*. This quantity can be derived from Mie theory calculations [4, 5], provided the complex index of refraction in the relevant ir wavelength region, the bulk density and the geometrical proportions of the structural elements are known. A second possibility to determine the effective specific extinction is to perform spectral ir-optical directional-hemispherical transmission and reflection measurements [11] and to use the three-flux-approximation of the equation of radiation transport. For an optically infinite thick specimen the reflection data provide the albedo $\omega^*(\Lambda)$, i.e. the ratio between scattering and extinction coefficient. From the albedo and the transmission measurements the mass-specific effective extinction $e^*(\Lambda)$ is deduced. The temperature dependence of $e^*(\Theta)$ can be determined from proper averaging of $e^*(\Lambda)$ over the thermal spectrum, using the Rosseland weighting function. Typical specific extinctions for foams are in the range from 30 to 60 m^2 kg^{-1} at 300 K. Using these data the radiative conductivity for a mean temperature Θ_m can be calculated from the equation

$$\lambda_r = \frac{16}{3} \cdot \frac{n^2 \sigma}{e_R^*(\Theta_m)\rho} \cdot \Theta_m^3. \qquad (7)$$

Typical values of $\lambda_r \approx 0.004$–0.007 W m^{-1} K^{-1} result for a foam with $\rho = 40$ kg m^{-3} at $\Theta_m = 300$ K.

3. RESULTS

3.1. *Specimens*

Several foams with closed cell structure have been investigated. Here only results for

a CFC-blown extruded polystyrene foam (PS) ($\rho = 34$ kg m^{-3});

an R 11-blown rigid polyurethane foam (PU1) ($\rho = 48$ kg m^{-3}) without surface diffusion barriers aged for 8 months; and

a freshly R 11-blown rigid PU foam (PU2) ($\rho = 30$ kg m^{-3})

are presented in order to discuss the most important features of thermal transport. Emphasis is put on a quantitative description of the radiative transfer. Especially for the PS foam detailed calculations are performed to discuss the influence of the foam structure on the specific extinction. For PU2 only the ir data are presented as an example for a low density PU foam.

3.2. *Ir-optical properties*

3.2.1. *Polystyrene foam.* In order to determine the spectral complex index of refraction $m(\Lambda) = n(\Lambda) + ik(\Lambda)$ we prepared non-porous PS films (thicknesses from 20 to 500 μm) in a heated press. Typical temperatures were 120°C. From directional–directional transmission measurements a first order imaginary part $k_1(\Lambda)$ of the complex index of refraction is determined. The 'subtractive Kramers–Kronig relation' [12] allows one to calculate $n_1(\Lambda)$. Comparison between a measured transmission T and a computed $T(n_1, k_1)$ yields an improved value k_2. This procedure is performed iteratively until $T(n_n, k_n)$ is in good agreement with the measured transmission [13].

The data shown in Fig. 3 allow one to calculate the scattering phase function and the spectral relative extinction cross-section Q^* for the struts as well as for the walls. Here the walls are taken as randomly

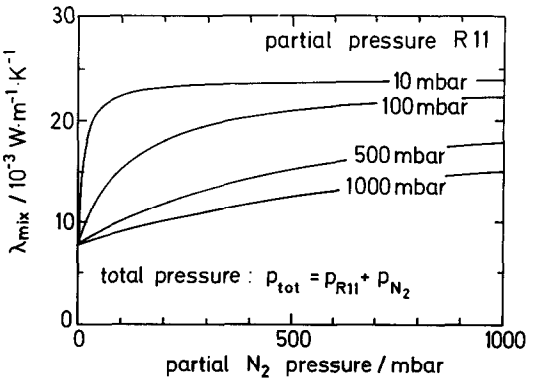

FIG. 2. Increase of total gaseous conductivity λ_{mix} for an R 11/nitrogen mixture versus partial nitrogen pressure p_N; the partial pressure p_{R11} of R 11 is the parameter.

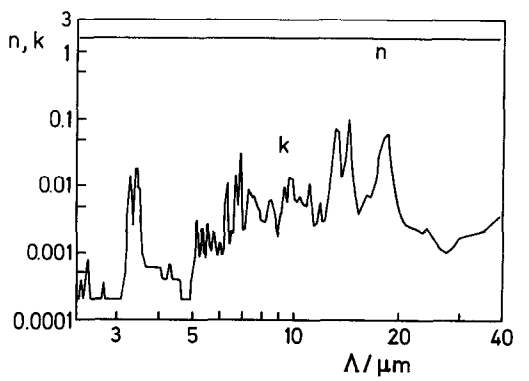

FIG. 3. Components n and k of the complex index of refraction $m(\Lambda) = n + ik$ versus wavelength Λ for polystyrene [13].

oriented platelets, whereas infinitely long cylinders are used to describe the struts. In the latter case the triangular cross-sections are converted into circular ones with the same geometrical mean cross-section. The random orientation of these cylinders with respect to the impinging radiative flux is taken into account in the Mie scattering calculations.

From the spectral relative extinction cross-section $Q^*(\Lambda)$ the spectral specific extinction

$$e^*(\Lambda) = \gamma/\rho_0 \cdot Q^*(\Lambda) \tag{8}$$

is determined, where

$$\gamma = \begin{cases} 4/(\pi \cdot \phi) & \text{for cylinders} \\ 1/\delta & \text{for platelets.} \end{cases}$$

In the case of platelets, Q^* can be calculated from Fresnel's equations by use of the reflection $R(\alpha, n, k)$ and the transmission $T(\alpha, n, k)$ of a slab:

$$Q^* = \int_0^{\pi/2} [R(\alpha, n, k) \cdot \cos(2\alpha) + 1 - T(\alpha, n, k)] \cdot 1/2 \sin(2\alpha)\, d\alpha. \tag{9}$$

α is the angle between the impinging radiation and the normal of the platelets. Afterwards $Q^*(\Lambda)$ or $e^*(\Lambda)$ are Rosseland-averaged. The results in dependence of the geometry are shown in Figs. 4 and 5 for three temperatures. As can be seen, the variation of e^* with δ at a constant temperature is rather weak, whereas the variation of e^* with ϕ_s is remarkable; an optimal diameter is $\phi_s \approx 5\ \mu m$.

A total specific extinction e^*_{tot} can be calculated using the mass fractions f_s and f_w. For the PS foam investigated (Table 1), we get at $\Theta \approx 300$ K

$$\begin{aligned} e^*_{tot} &= 0.7 e^*_s(\phi_s = 7\,\mu m) \\ &\quad + 0.3 e^*_w(\delta = 0.9\,\mu m) \\ &= (0.7 \cdot 74 + 0.3 \cdot 60)\,m^2\,kg^{-1} \\ &= 70\,m^2\,kg^{-1}. \end{aligned} \tag{10}$$

For commercially available PS foams one can generally conclude that the struts provide most of the specific extinction. The measured spectral specific extinction $e^*(\Lambda)$ is shown in Fig. 6. Typical for PS are firstly the decrease of e^* with Λ and secondly the occurrence of a 'quartet' between 5 and 6 μm, caused by CH vibrations.

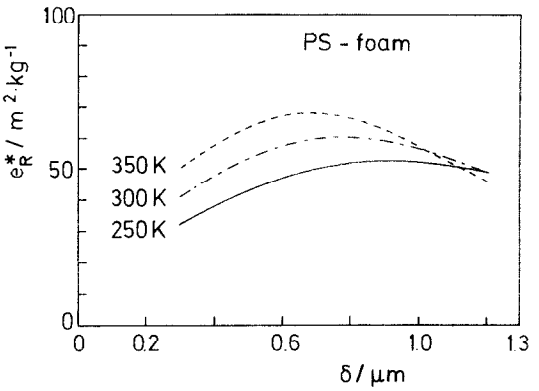

FIG. 5. Effective specific extinction coefficient e^*_R for platelets (walls) versus thickness δ for 250, 300 and 350 K. Calculated with Mie theory and $m(\Lambda)$ from Fig. 3.

From the measured spectral dependence the Rosseland-averaged specific extinction is derived (Fig. 7). The agreement between these values and the data from the Mie scattering calculations according to equation (10) is within 10%. The calculated values are higher than those from experiments, because dependent scattering of radiation is not considered in the Mie theory. In reality this effect occurs because the walls and struts are in physical contact [14]. The radiative conductivity for the PS foam with $\rho = 34$ kg m^{-3} is around 0.0046 W m^{-1} K^{-1} at 300 K.

The albedo is depicted in Fig. 8; it agrees well with data from ref. [15]. The major part of the extinction is obviously provided by scattering.

3.2.2. *Polyurethane foam.* In the case of polyurethane it is not possible to derive the spectral complex index of refraction $m(\Lambda)$ in the same manner as for PS foam, because PU is not thermoplastic. As thin foils of the same PU material investigated were not available, we refrain from a determination of $m(\Lambda)$.

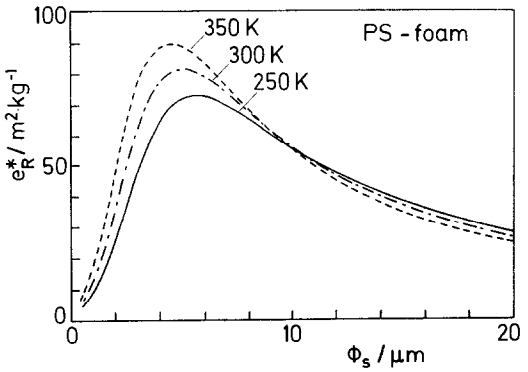

FIG. 4. Effective specific extinction coefficient e^*_R for cylinders (struts) versus diameter ϕ_s for 250, 300 and 350 K. Calculated with Mie theory and $m(\Lambda)$ from Fig. 3.

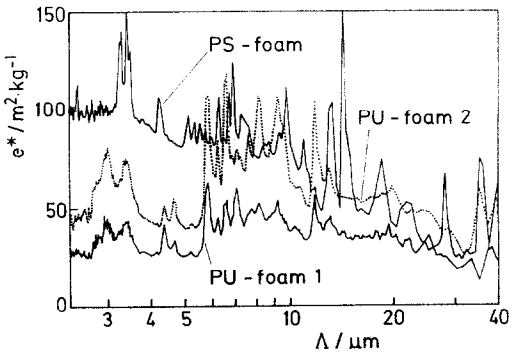

FIG. 6. Measured spectral extinction $e^*(\Lambda)$ for the PS and the PU foams versus wavelength.

Table 1. Properties of the investigated PU and PS foams

	PU1	PU2	PS
ρ (kg m^{-3})	48	30	34
ρ_0 (kg m^{-3})	1230	1230	1150
λ_0, 300 K (W m^{-1} K^{-1})	0.26	0.26	0.23
ϕ_c (μm)	164	230	84
ϕ_s (μm)	c. 2.0	c. 15	7.0
δ (μm)	c. 1.5	c. 1.0	0.9
f_s	c. 0.85	c. 0.72	0.67
Photographs taken with	optical microscope	optical microscope	SEM
e_R^*, 300 K (m^2 kg^{-1})	35	61	60
λ_s, 300 K (W m^{-1} K^{-1})	0.0039	0.0027	0.0030
λ_r, 300 K (W m^{-1} K^{-1})	0.0050	0.0046	0.0041
λ, 300 K (W m^{-1} K^{-1})	0.025	0.018	0.026
Aged	8 months	2 weeks	8 months
At temperature	300 K	300 K	300 K
Surface covers during storage	no	yes	no

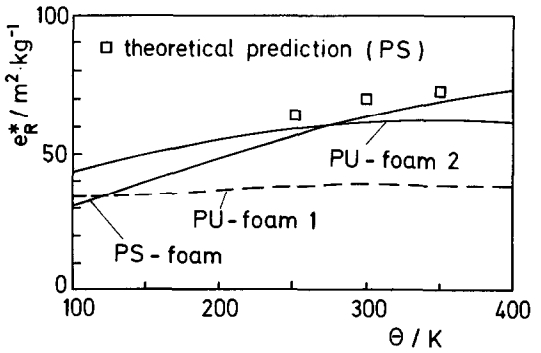

FIG. 7. Rosseland-averaged specific extinction e_R^* of the PS foam as a function of temperature Θ.

which is necessary to perform calculations with the Mie theory, and to determine the influence of the structure on the specific extinction $e_R^*(\Theta)$. Thus we derive $e_R^*(\Theta)$ experimentally for several PU foams with various densities to demonstrate the correlation between structure and specific extinction. Here two examples for the lower and upper cases are given.

The spectral specific extinction $e^*(\Lambda)$ for the PU foam 1 ($\rho = 48$ kg m^{-3}) (Fig. 6), obtained from directional-hemispherical transmission and reflection measurements is about 35–40 m^2 kg^{-1} with some fluctuation about the mean value. PU foam 2 ($\rho = 30$ kg m^{-3}) shows a similar dependency of extinction on wavelength as PU foam 1 in Fig. 6. However, the absolute value of e^* of the low density PU foam 2 is, on average, nearly a factor 2 higher than for PU foam 1. Also, the absorption peaks are more pronounced for PU foam 2, because the radiation interacts more effectively with the especially filigrane foam structures.

According to Fig. 6 the Rosseland-averaged extinction values of the PU foams (Fig. 7) depend only weakly on temperature. However, significant differences in their mean values are observed. At $\Theta =$ 300 K the $\rho = 30$ kg m^{-3} PU foam 2 has an $e_R^*(\Theta)$ value of 61 m^2 kg^{-1}, which exceeds the value of PU foam 1 ($e_R^* = 35$ kg m^{-2}) by about 75%. This corresponds to a radiative conductivity for PU foam 1 of 0.0050 W m^{-1} K^{-1} at 300 K and 0.0046 W m^{-1} K^{-1} for PU foam 2.

The albedo ω^* (Fig. 8) is large ($\approx$0.6) for wave-

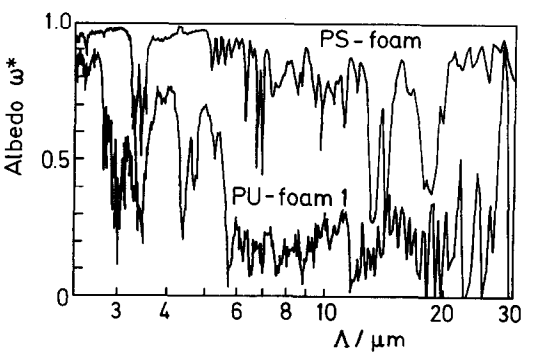

FIG. 8. Spectral variation of the albedo ω^* of the PS and the PU foam ($\rho = 48$ kg m^{-3}).

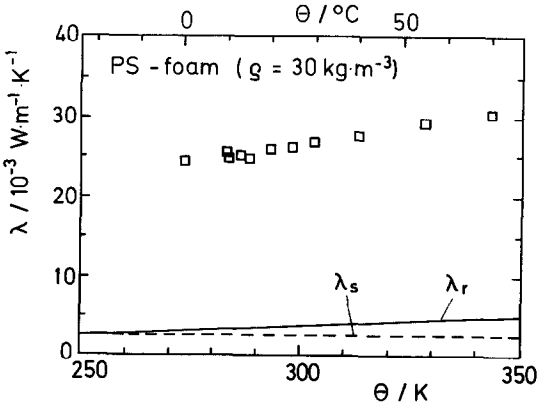

FIG. 9. Thermal conductivity of a PS foam with $\rho = 34$ kg m^{-3}, aged at room temperature for about 8 months versus temperature Θ; solid and radiative thermal conductivities λ_s and λ_r, respectively, are depicted.

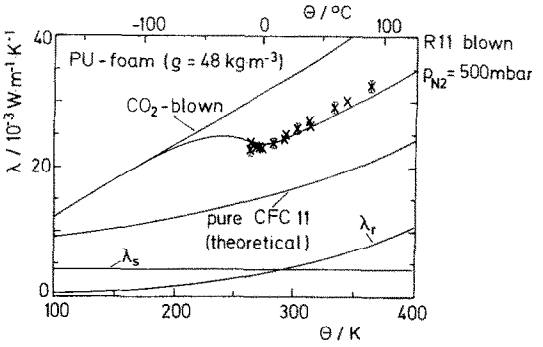

FIG. 10. Total thermal conductivities λ for a PU foam ($\rho = 48$ kg m^{-3}) versus temperature Θ. (——) Model calculations; ($\times\times\times$) measurements for an R 11-blown PU foam after 8 months of aging at room temperature. In the case of the CO_2-blown foam the cells are assumed to contain only N_2. At the bottom of this figure radiative and solid conductivities λ_r and λ_s, respectively, are also depicted.

lengths below 6 μm and small (≈ 0.2) for $\Lambda > 6$ μm. Thus we hesitate to accept Glicksman and Torpey's approach [16], to derive the extinction from simple directional–directional transmission measurements. Deviations are of the order of 100%, which are caused predominantly by scattering in the $\Lambda < 6$ μm region.

3.3. *Caloric measurements of the total conductivity*

Caloric conductivity data are collected with guarded hot plate devices in the temperature range 250–350 K. The specimens investigated are cut from the middle of rigid foam blocks with thicknesses from 1.5 to 2.5 cm.

3.3.1. *Polystyrene foam.* The calorimetrically determined total conductivity is presented in Fig. 9. Additionally calculated solid and radiative conductivities are depicted. The latter were derived from equations (5) and (7), as well as from the geometrical data from Table 1 and the specific extinction $e_R^*(\Theta)$ shown in Fig. 7.

At 300 K a solid conductivity of 0.003 W m^{-1} K^{-1} and a radiative conductivity of 0.004 W m^{-1} K^{-1} are predicted. As the measured total conductivity is about 0.026 W m^{-1} K^{-1}, the gaseous conductivity can be estimated to be about 0.019 W m^{-1} K^{-1}. Condensation effects similar to the PU foam (see Fig. 10) are not observed, because the PS foam is mainly blown with R 12 (CF_2Cl_2), which has a lower boiling point than R 11. The exact composition of the cell gas is not known to the authors. Thus the gaseous conductivity cannot be predicted.

3.3.2. *Polyurethane foam.* In the case of the PU foam the experimental data are compared with calculations for various R 11/N_2 ratios. Results for an aged PU foam are shown in Fig. 10; they coincide well with the 500 mbar model curve, which is calculated from equations (1), (5), (6) and (7). Equation (6) is modified with respect to condensation effects. The temperature-dependent pressures p_1 and p_2 in the constant volume of a foam cell either describe the law of a real gas or the vapour pressure curve. It is noteworthy that a plateau or a relative maximum of the total conductivity is expected between 200 K and 250 K, which can be explained by a partial condensation of the R 11 gas within the pores. This causes an increase of the gaseous conductivity with decreasing temperature.

The calorimetric results and the calculated curves in Fig. 10 and the data in Table 1 quantify the well-known fact that aging causes a steady increase of λ_g and thus also of λ with time: $\lambda \approx 0.018$ W m^{-1} K^{-1} (freshly blown) versus $\lambda \approx 0.025$ W m^{-1} K^{-1} (aged for 8 months) at 300 K. The same foam, blown with CO_2, would have a conductivity $\lambda \approx 0.035$ W m^{-1} K^{-1} after a few days.

In Fig. 10 the solid and radiative thermal conductivities are depicted. For the PU foam with $\rho = 48$ kg m^{-3} these mechanisms contribute with 0.004 and 0.005 W m^{-1} K^{-1} at 300 K to the total thermal conductivity.

In general, for higher temperatures the radiative conductivity becomes even more important, whereas λ_s has only a weak temperature dependence. The examples discussed in this report demonstrate the influence of density and structure on the combined solid and radiative conductivity, which contributes between 0.006 and 0.010 W m^{-1} K^{-1} to the total thermal conductivity at 300 K (Table 1).

4. OUTLOOK

It has been shown that the radiative transport in foams can be reliably described if either the complex index of refraction, the bulk density and the geometrical proportions are known and/or if directional–hemispherical transmission and reflection measurements are performed. Directional–directional transmission data are not sufficient.

Substitution of environmentally harmful blowing agents generally leads to a remarkable increase in conductivity: with CO_2 a 45% higher thermal conductivity is observed than with R 11 after 8 months of aging. This percentage can be reduced to 5 or 11%, respectively, when R 123 (CF_3–$CHCl_2$) or R 141b (CCl_2F–CH_3) are used [17].

The foam industry also investigates water-blown foams: the cell gas in this case is mainly CO_2, which is known to diffuse rather quickly through the foam membranes. An improvement may be possible if surface diffusion barriers are used.

To compensate for the degradation of thermal performance, foams can be used to sandwich highly effective thermal insulants, such as vacuum sealed aerogel or fumed silica panels [18]. The foams in these constructions primarily serve as fillers, gluing agents and mechanical stabilizers, while the evacuated panels provide most of the thermal resistance.

Acknowledgements—We are indebted to Bayer AG, Leverkusen and BASF/Lugwigshafen for generously pro-

viding foam samples and to the German BMFT for financial support of this project.

REFERENCES

1. L. R. Glicksman and M. R. Torpey, Factors governing heat transfer through closed cell foam insulation, *ASTM Symposium*, Florida (1987).
2. L. M. Zwolinski, Foam insulation aging: historical perspective and outstanding problems. In *Insulation Materials, Testing and Applications* (Edited by D. L. McElroy and J. F. Kimpflen), pp. 189–196. American Society for Testing and Materials, Philadelphia (1990).
3. A. G. Ostrogorsky, L. R. Glicksman and D. W. Reitz, Aging of polyurethane foams, *Int. J. Heat Mass Transfer* **29**, 1169–1176 (1986).
4. H. C. van de Hulst, *Light Scattering by Small Particles*. Wiley, New York (1957).
5. B. Parr, IR-Reflexionsmessungen zur Bestimmung von optischen Konstanten und Schichtdicken, Diploma Thesis, Univ. Würzburg (1988).
6. R. Caps, K. Baumeister and J. Fricke, Radiative transfer in thermal insulations of low optical density, *High Temperatures–High Pressures* **18**, 589–597 (1986).
7. M. Bomberg and D. A. Brandreth, Evaluation of long-term thermal resistance of gas-filled foams: state of the art. In *Insulation Materials, Testing and Applications*, *ASTM STP* 1030 (Edited by D. L. McElroy and J. F. Kimpflen), pp. 156–173. American Society for Testing and Materials, Philadelphia (1990).
8. B. Koglin, Der Wärmetransport in Schaumstoffen, Thesis, TU Berlin (1967).
9. A. G. Ostrogorsky and L. R. Glicksman, Variation of insulating properties of closed cell foam insulation. In *Insulation Materials, Testing and Applications* (Edited by D. L. McElroy and J. F. Kimpflen), pp. 109–120. American Society for Testing and Materials, Philadelphia (1990).
10. A. Wassiljewa, Wärmeleitung in Gasgemischen, *Phys. Z.* **5**(22), 737 (1904).
11. J. Fricke *et al.*, Optically thin fibrous insulations. In *Insulation Materials, Testing and Applications* (Edited by D. L. McElroy and J. F. Kimpflen), pp. 575–586. American Society for Testing and Materials, Philadelphia (1990).
12. R. K. Ahrenkiel, Modified Kramers–Kronig analysis of optic spectra, *J. Opt. Soc. Am.* **61**(12), 1651 (1971).
13. H.-P. Ebert, Strahlungsbezogene Optimierung von Wärmedämmungen, Diploma Thesis, Univ. Würzburg (1990).
14. H. C. Hottel *et al.*, Optical properties of coatings. Effect of pigment concentration, *AIAA J.* **9**, 1895–1898 (1971).
15. S. Yajnik and J. A. Roux, Spectral radiative properties and apparent thermal conductivity of expanded polystyrene foam insulation, *ASTM Symposium*, Florida (1987).
16. L. R. Glicksman and M. R. Torpey, The influence of cell size and foam density on the thermal conductivity of foam insulations, *Polyurethane World Congress* (1987).
17. J. E. Christian *et al.*, The technical viability of alternative blowing agents in polyisocyanate roof insulation, Part 3, *In situ* thermal aging and performance in different roof systems, *33rd Annual Polyurethane Technical Marketing Conf.*, pp. 247–259 (1990).
18. J. Fricke *et al.*, Opaque silica aerogel insulations as substitutes for polyurethane foams, *21st Int. Therm. Cond. Conf.*, Lexington (1989).

TRANSPORT THERMIQUE DANS LES MOUSSES ISOLANTES DE POLYSTYRENE ET DE POLYURETHANE

Résumé—Le transport thermique dans les mousses isolantes de polystyrène (PS) et de polyuréthane (PU) est décrit avec un regard particulier sur le transfert radiatif. Des mesures calorimétriques de la conductivité totale sont faites à l'aide de la plaque chaude gardée. Les propriétés radiatives des mousses sont déduites d'études optiques infrarouges avec un spectromètre FTIR. Dans le cas de la mousse PS, les propriétés radiatives sont aussi tirées de calculs par la théorie de Mie pour les cylindres infinis et les plaques représentant la configuration des cellules de la mousse. On modélise la conductivité thermique totale des mousses PU, incluant les effets de la condensation sur l'agent de soufflage R11.

WÄRMETRANSPORT IN ISOLIERSCHÄUMEN AUS POLYSTYROL UND POLYURETHAN

Zusammenfassung—Es wird der Wärmetransport in Isolierschäumen aus Polystyrol (PS) und Polyurethan (PU) beschrieben unter besonderer Berücksichtigung des Strahlungswärmetransports. In einer Plattenapparatur mit Schutzheizung werden kalorische Messungen der Gesamtwärmeleitfähigkeit ausgeführt. Die Strahlungseigenschaften der Schäume werden aus infrarot-optischen Untersuchungen mit Hilfe eines FTIR-Spektrometers ermittelt. Im Falle des PS-Schaums werden die Strahlungseigenschaften zusätzlich aus Berechnungen bestimmt. Hierbei wird die Mie-Streuungstheorie auf unendliche Zylinder und Plättchen angewandt, die die Struktur der Schaumzellen darstellen. Die Gesamtwärmeleitfähigkeit des PU-Schaums wird unter Einbeziehung der Kondensation des Blähmittels R11 modelliert.

ПЕРЕНОС ТЕПЛА В ИЗОЛЯЦИИ ИЗ ПОЛИСТИРОЛОВОЙ И ПОЛИУРЕТАНОВОЙ ПЕН

Аннотация—Описывается перенос тепла в изоляции из полистироловой и полиуретановой пен. Основное внимание обращено на лучистый перенос. Проведены калориметрические измерения суммарной теплопроводности в пластинчатом термоанемометре. С помощью оптических спектрометрических измерений определены лучистые характеристики пен. Кроме того, для полистироловой пены лучистые характеристики рассчитаны по теории рассеяния Ми для бесконечных цилиндров и пластинок, которыми моделируются прослойки и стенки ячеек пены. Определена суммарная теплопроводность полиуретановых пен, включая эффекты конденсации вдуваемого фреона 11.